JOURNAL OF GEOPHYSICAL RESEARCH, VOL. 105, NO. C7, PAGES 16,999–17,010, JULY 15, 2000

Undertow over a barred beach

A. F. Garcez Faria,[1] E. B. Thornton, T. C. Lippmann,[2] and T. P. Stanton
Oceanography Department, Naval Postgraduate School, Monterey, California

Abstract. The spatial distribution of the mean cross-shore flow (undertow) over a barred beach is examined with field data obtained on three energetic wave days during the Duck94 experiment. The vertical structure of the undertow is modeled using a turbulent eddy viscosity closure and includes the important effects of wave breaking (described using the roller concept) and convective acceleration of the current. Other than a more realistic description of observed turbulence variations, a depth-dependent eddy viscosity (compared with a constant) does not improve the agreement between predicted and observed undertow profiles. The effect of using different boundary conditions is investigated by extending the formulations of *Stive and Wind* [1986] and *Svendsen et al.* [1987] to include random waves by ensemble averaging over the wave height distribution. The contribution of breaking wave rollers to the surface mass flux can be of the same order or greater than the contribution associated with the organized wave motion. The largest discrepancies between model predictions and observations occur over the sandbar, where the mass transport of the breaking waves appears to be underestimated.

1. Introduction

The local vertical imbalance between the wave setup pressure gradient, which is uniform with depth, and the depth-varying wave radiation stress is conceptually responsible for driving the undertow [*Dyhr-Nielsen and Sørensen*, 1970]. In the past 2 decades several theoretical models for the vertical structure of the undertow for two-dimensional beaches have been developed [e.g., *Svendsen*, 1984; *Dally and Dean*, 1984; *Stive and Wind*, 1986; *Deigaard et al.*, 1991; *Haines and Sallenger*, 1994]. All models use an eddy viscosity closure scheme and solve for the depth-dependent undertow by integrating the cross-shore momentum equation twice over depth, which requires two boundary conditions to evaluate the integration constants.

There is a general consensus throughout the literature of using local conservation of mass over the vertical as one boundary condition. Commonly, the second boundary condition is either the stress at the trough level [*Stive and Wind*, 1986] or the no-slip condition at the bottom combined with the steady streaming generated by the bottom boundary layer (BBL) [*Svendsen*, 1984]. Despite significant physical differences both approaches reduce to the same form between the trough level and the top of the bottom boundary layer within the surf zone as contributions from steady streaming and bed shear stress are outweighed by mean water slope and wave forcing gradients.

The wave-induced onshore mass flux in the region between the wave crest and trough is critical to predicting the magnitude of the undertow, which is predicted heuristically by adding the contribution from breaking wave rollers to the mass transport given by an irrotational wave theory [*Svendsen*, 1984]. *Dally and Brown* [1995], found better agreement for laboratory-generated regular waves breaking over a planar beach using stream function theory [*Dean*, 1974] than the linear wave theory, which tended to overpredict the depth-averaged undertow. On the other hand, *Masselink and Black* [1995], using field measurements from experiments at two planar beaches, found good agreement using shallow water linear wave theory.

Most existing undertow models show good agreement with laboratory data for monochromatic waves breaking over planar beaches when the depth-averaged mean return flow is adjusted to fit the data (instead of using predicted mass flux) and the magnitudes of the two largest dynamical forcing terms (wave setup and radiation stress gradients) are determined from data. Validation of these models with field data has been limited by the lack of data. *Smith et al.* [1992] compared an undertow model to data from the 1990 Delilah experiment performed at the same Duck, North Carolina, beach studied here and found large discrepancies over the bar, where the model underpredicted observed velocities. This strong "undertow jet" over the bar was also observed during an earlier field experiment [*Haines and Sallenger*, 1994] at the same site.

Within the surf zone, wave breaking–generated turbulence dominates bottom boundary layer processes, with the turbulent shear stress maximum at the surface and decreasing toward the bottom. *Ting and Kirby* [1994], using laser Doppler velocimetry (LDV) data from a wave flume experiment, found that the primary turbulence-generating mechanism in the surf zone is due to wave breaking at the wave-roller interface and that turbulence intensities decrease with distance from the surface. *Cox and Kobayashi* [1997], using laboratory LDV measurements of regular, spilling breakers on a rough plane slope, observed that the shear stress distribution within the surf zone varies linearly with depth until the top of the (BBL) and that the eddy viscosity μ_z is small near the trough level, increases to a maximum about one-third of the depth below the trough level, and then decreases toward the bottom. *Svendsen* [1984] investigated the effect of introducing an exponentially varying μ_z to the predicted vertical profile of the undertow. In his formulation, two free parameters are necessary to define the

[1]Now at Marinha-Directoria de Hidrografiea e Navegacao, Rio de Janeiro, Brazil.
[2]Now at Byrd Polar Research Center, Ohio State University, Columbus.

Paper number 2000JC900084.

magnitude and decay rate with depth of μ_z, and despite the more realistic depth variation of μ_z, only marginal improvements are obtained for the vertical profile of the undertow [*Svendsen and Buhr Hansen*, 1988].

In this paper, field observations of vertical profiles of the mean cross-shore current obtained over a barred beach are used to test various models. Wave height transformation is based on an energy flux balance including the effects of rollers to describe wave breaking and a probabilistic description of wave heights. The surface mass flux is investigated using both linear and higher-order wave theories and includes the contribution from surface rollers. The influence of depth-dependent formulations for the eddy viscosity and different choices of boundary conditions on the vertical structure of the undertow are examined.

2. Theory

A right-handed coordinate system with origin at the shoreline (x positive offshore) and z positive upward from the sea surface is used. Solutions for the surface mass flux, the setup, and the vertical profile of the undertow are described assuming stationary wave conditions, straight and parallel depth contours, and random waves that are narrowbanded in both frequency and direction.

2.1. Wave Transformation

Wave transformation is determined using a probabilistic breaking wave model that includes roller energy gradients in the energy flux balance [*Lippmann et al.*, 1996]. This model assumes that wave heights both inside and outside the surf zone can be reasonably described by the Rayleigh distribution [*Thornton and Guza*, 1983] and gives accurate results for random waves breaking over both planar and barred beaches. The model has two free parameters: σ, the mean angle of the wave-roller interface, and γ, a measure of breaking wave intensity. Although the model is insensitive to the interfacial angle (kept constant at $\sigma = 10°$ for all runs) based on model results obtained by *Lippmann et al.* [1996] at the same location of the Duck94 experiment, adjusting γ to fit the data is unnecessary.

Wave properties are ensemble-averaged by integrating wave heights through the assumed Rayleigh distribution $p(H)$. Following *Thornton and Guza* [1983], the fraction of waves that are breaking is found by integrating through the breaking wave distribution $p_b(H) = W(H)p(H)$, where $W(H)$ is a weighting function (T. C. Lippmann and E. B. Thornton, The spatial distribution of wave breaking on a barred beach, submitted to *Journal of Geophysical Research*, 1998, hereinafter referred to as Lippmann and Thornton, submitted manuscript, 1998).

2.2. Surface Mass Flux

The conservation of mass for straight and parallel contours with the no-flow boundary condition through the beach is given by

$$\overline{\int_{-h}^{\eta} \rho[U(z) + \tilde{u}(z) + \acute{u}(z)]\, dz} = 0, \tag{1}$$

where the overbar indicates time averaging; η is surface elevation; h is the local water depth; ρ is water density; and onshore horizontal velocity has been partitioned into mean, wave, and turbulence contributions. In a Eulerian reference frame and assuming irrotational flow below the trough level, there is a net shoreward mean mass transport by waves limited to an upper region between the crest and trough that is given by

$$q_w = \overline{\int_{\eta_t}^{\eta_c} \rho\tilde{u}(z)\, dz}, \tag{2}$$

where the subscripts c and t refer to the crest and trough.

An additional contribution to the mass transport (per crest width) occurs above the wave trough (surface layer) that arises from the presence of turbulent wave rollers [*Svendsen*, 1984] and is defined by

$$q_r = \rho_r A \frac{c}{L}, \tag{3}$$

where ρ_r is the roller density, A is the roller cross-sectional area, L is the wavelength, and c is the advection velocity of the roller, assumed to be given by the wave phase speed. The roller contribution (3) to the surface mass flux is based on the calculated cross-sectional area of the roller. Earlier models [*Svendsen*, 1984; *Deigaard et al.*, 1991] assumed that this area is proportional to the rms wave height. As a consequence, the largest mean return flow would be predicted to occur at the breaker point, which is contrary to laboratory observations [*Nadaoka and Kondoh*, 1982]. *Dally and Brown* [1995] solve for the area of the roller for the case of monochromatic waves breaking over a planar beach by simultaneously solving the depth-integrated and time-averaged energy, continuity, and cross-shore momentum equations and found good agreement with existing laboratory data. However, their model requires observations of the cross-shore distribution of either the mean return flow or the setup to constrain the model and therefore cannot be applied to the present data.

Another recent roller model (Lippmann and Thornton, submitted manuscript, 1998) presents an independent method for calculating q_r and is calibrated using video observations to determine the cross-shore variation of the fraction of waves that are breaking. This model is based on the energy flux balance and describes energy dissipation following *Deigaard* [1993]. Two free parameters in the model, B, the vertical fraction of wave height covered by the roller, and ψ, a measure of the average wave face angle, are adjusted to give a rms best fit to breaking observations.

The onshore mass transport in the upper region is assumed to be balanced locally by a mean return flow below the trough (undertow):

$$q_w + q_r = -\overline{\int_{-h}^{\eta_t} \rho U(z)\, dz} = -\rho U_r h_t, \tag{4}$$

where U_r is the depth-averaged return flow, and h_t is the depth below the trough. The assumption that the undertow is limited to the region below the trough will be shown, in general, to be a reasonable assumption.

2.3. Undertow

The time-averaged cross-shore momentum equation, neglecting molecular viscous stresses and assuming straight and parallel contours and stationary wave conditions, is given by

$$\frac{\partial \rho \overline{u^2}}{\partial x} + \frac{\partial \rho \overline{uw}}{\partial z} = -\frac{\partial \bar{p}}{\partial x}. \quad (5)$$

The horizontal and vertical velocities (u and w) are expanded into mean, turbulent, and wave-induced components, $u = U + \acute{u} + \tilde{u}$ and $w = \acute{w} + \tilde{w}$, where the mean vertical velocity is assumed negligible (on a sloping bed, there will be a near-bed mean vertical current when a current is present to satisfy the impermeability condition). The time-averaged pressure, $\bar{p} = \rho[g(\bar{\eta} - z) - \overline{\tilde{w}^2} - \overline{\acute{w}^2}]$, is obtained from the vertically integrated vertical momentum equation, after neglecting contributions from the cross-shore gradient of the vertically integrated wave and turbulent shear stress [*Stive and Wind*, 1982]. After substituting for the time-averaged pressure, (5) can be further simplified for the region between the top of the BBL and the trough level (middle layer) with the aid of the following assumptions: (1) wave and turbulent velocity components are statistically independent; (2) turbulence is near isotropic, $\overline{\acute{u}^2} \simeq \overline{\acute{w}^2}$ [*Stive and Wind*, 1982]; (3) the wave shear stress is given by [*Rivero and Arcilla*, 1995]

$$\frac{\partial \rho \overline{\tilde{u}\tilde{w}}}{\partial z} = -\frac{1}{2}\frac{\partial}{\partial x}\rho[\overline{\tilde{u}^2} - \overline{\tilde{w}^2}];$$

and (4) a first-order eddy viscosity closure for the turbulent shear stress is given by $-\rho \overline{\acute{u}\acute{w}} = \rho \mu_z (\partial U/\partial z)$. Applying these assumptions, (5) reduces to

$$\frac{\partial}{\partial z}\left(\rho \mu_x \frac{\partial U}{\partial z}\right) = \frac{1}{2}\frac{\partial}{\partial x}[\rho(\overline{\tilde{u}^2} - \overline{\tilde{w}^2})] + \rho g \frac{\partial \bar{\eta}}{\partial x} + \frac{\partial \rho U_r^2}{\partial x}$$

$$= F(x), \quad (6)$$

where μ_z is the time-invariant turbulent eddy viscosity and the advection of mean cross-shore momentum has been approximated by $\rho U^2(z) \simeq \rho U_r^2$. The forcing $F(x)$ in (6) is due to the cross-shore gradients of radiation stress, setup (setdown), $\bar{\eta}$, and convective acceleration of the depth-averaged undertow. $F(x)$ can be assumed to be independent of elevation on the basis of empirical evidence from laboratory studies [*Nadaoka and Kondoh*, 1982; *Stive and Wind*, 1982, 1986] or to be more restrictive, limiting the discussion to long waves.

A solution for the vertical distribution of the mean undertow can be determined by integrating (6) twice over depth to give

$$U(z) = F(x)\int \frac{z}{\rho u_z}\, dz + C_1(x)\int \frac{dz}{\rho \mu_z} + C_2(x), \quad (7)$$

where $C_1(x)$ and $C_2(x)$ are integration coefficients. Both the *Stive and Wind* [1986] and *Svendsen et al.* [1987] solutions are used, with modifications to their original developments to improve the derivation. For both solutions, a different solution for the undertow forcing F was used as they wrongly assumed that the wave stress is small compared with the Reynolds stress ($\rho \overline{\tilde{u}\tilde{w}} \ll \rho \overline{\acute{u}\acute{w}}$), resulting in an overestimation of the forcing by [*Rivero and Arcilla*, 1995]

$$\frac{1}{2}\frac{\partial}{\partial x}\rho[\overline{\tilde{u}^2} - \overline{\tilde{w}^2}].$$

Here (6) will be used instead.

Although different formulations for the eddy viscosity variation with depth are investigated (appendix), the simplest solution for a depth-independent eddy viscosity μ is outlined here. For this case, (7) simplifies to

$$U(z) = \frac{1}{2\rho\mu}F(x)z^2 + \frac{1}{\rho\mu}C_1(x)z + C_2(x). \quad (8)$$

First, following *Stive and Wind* [1986], $C_1(x)$ is determined by integrating (6) once over depth and solving for the shear stress at the trough level, and $C_2(x)$ is found by applying conservation of mass over the vertical (see Appendix for details) to give

$$U(z) = U_r + \frac{1}{\rho\mu}F(x)[A_0 + A_1 + A_2 z^2] + \frac{\bar{\tau}_{bx}}{\rho\mu}\left[z + h - \frac{h_t}{2}\right], \quad (9)$$

where $\bar{\tau}_{bx}$ is the mean cross-shore bed shear stress that is calculated using a quadratic formulation ($\bar{\tau}_{bx} = \rho C_f |\overline{\tilde{u}_b}| U_b$, where $C_f = 0.01$ is a constant friction factor and $\tilde{u}_b$ is the near-bottom wave-induced velocity). This solution is a second-degree polynomial in z with coefficients

$$A_0 = \frac{1}{2},$$

$$A_1 = h,$$

$$A_2 = \frac{3h^2 - h_6^2}{6}.$$

The solution (9) has been previously applied to monochomatic waves and can be extended to random waves by ensemble averaging over the wave height distribution:

$$\langle U(z) \rangle = U_r + \frac{1}{\rho\mu}\int_0^\infty \left[(A_0 + A_1 z + A_2 z^2)F(x) + \bar{\tau}_{bx}\left(z + h\,\frac{h_t}{2}\right)\right] p(H)\, dH \quad (10)$$

The effect of $\bar{\tau}_{bx}$ is small compared with wave-breaking dissipation [*Thornton and Guza*, 1983; *Svendsen*, 1984; *Dally and Brown*, 1995], and hence the vertical structure of the undertow is mostly determined by the quadratic term. The amount of curvature in the vertical velocity profile is a function of both F (calculated from wave quantities) and the eddy viscosity μ. Large values of F produce more vertical shear, resulting in a parabolic profile, whereas large values of μ reduce the vertical shear, producing a more uniform velocity profile with depth. Differences from *Stive and Wind* [1986] are the inclusion of the momentum flux of the mean current term in the forcing, retaining the bottom shear stress, and treating of the waves as random requiring ensemble averaging.

The influence of the boundary condition choice on the vertical structure of the mean undertow is investigated by comparing the results obtained by (10) with the *Svendsen et al.* [1987] model that uses a no-slip condition at the bottom to replace the stress at the trough level as the second boundary condition. This no-slip condition is obtained by coupling the undertow model with a bottom boundary layer model. Within the BBL, the flow is a combination of the steady streaming induced by the oscillatory motion and the undertow above, which results in a mean velocity at the top of this layer (U_b) that is obtained by requiring continuity in velocity and shear stress between these two regions to give (see *Svendsen et al.* [1987] for details)

$$\langle U(z)\rangle = U_b + \frac{1}{\rho\mu}\int_0^\infty [(A_3 + A_1 z + A_2 z^2)F(x) + \langle \bar{\tau}_{bx} - \bar{\tau}_{bs}\rangle (z + h)]p(H)\, dH, \quad (11)$$

where $A_3 = h^2/2$ and $\bar{\tau}_{bs}$ is related to the steady streaming in the BBL:

$$\left(\bar{\tau}_{bs} = -\frac{1}{2}\rho\mu_{bl}\sqrt{\frac{\pi f}{\mu_{bl}}}\frac{\overline{u_b}^2}{\sqrt{gh}}\right),$$

where f is wave frequency and μ_{bl} is the eddy viscosity inside the BBL). This model further assumes that μ_{bl} is much smaller than the eddy viscosity in the middle layer, which was recently verified in a laboratory experiment using LDV [*Cox and Kobayashi*, 1997]. Following *Putrevu and Svendsen* [1993], the eddy viscosity inside the BBL is estimated by

$$\frac{\mu_{bl}}{h\sqrt{gh}} = 0.32\, C_f^2 \left(\frac{H}{h}\right)^2.$$

An objective is to determine values of μ appropriate for the surf zone by model fitting to the observations.

2.4. Setup

The setup gradient is a dominant driving force for the undertow. The setup is calculated by depth integrating the time-averaged cross-shore momentum equation (5) from the bottom to the mean water level to give

$$\frac{\partial S_{xx}}{\partial x} + \frac{\partial M_r}{\partial x} + \frac{\partial \rho U_r^2(\bar{\eta} + h)}{\partial x} = -\rho g(\bar{\eta} + h)\frac{\partial \bar{\eta}}{\partial x}, \quad (12)$$

where S_{xx} is the wave radiation stress [*Longuet-Higgins and Stewart*, 1964], $M_r = cq_r$ is the momentum flux associated with wave rollers, and the last term on the left-hand side is the momentum flux of the mean current of the depth-averaged undertow approximated by

$$\overline{\int_{-h}^{\eta} U^2\, dz} \simeq U_r^2(\bar{\eta} + h).$$

In the derivation of (12) the mean bed shear stress [*Longuet-Higgins and Stewart*, 1964] and the cross-shore wind stress (owing to small observed onshore winds in the data described later) are assumed to be negligible.

3. Data

Field measurements were acquired as part of the Duck94 experiment [e.g., *Garcez Faria et al.*, 1998] conducted at the U.S. Army Corps of Engineers Field Research Facility (FRF) in Duck, North Carolina. The data selected for analysis are from October 10–12 when strong cross-shore currents (0.05–0.4 m s^{-1}) associated with a storm were present.

The vertical structure of the current was measured with a vertical stack of seven two-component Marsh-McBirney electromagnetic current meters (ems) mounted on a mobile sled at elevations 0.4, 0.7, 1.0, 1.5, 1.8, 2.2, and 2.6 m above the bed. The ems were horizontally displaced at least 1 m from the sled and oriented such that the vertical stack was in the updrift direction of the longshore current to minimize interference by the sled structure. The ems offsets were determined in situ and found to be repeatable to within 1 cm s^{-1}. The sled orientation was determined using a digital compass mounted on the sled with accuracy O(1°). Measured two-component velocities were rotated to a shore normal right-handed coordinate system using compass data and adding at each sled position any deviation of the bottom contour line from a shore parallel direction. Determination of the rotation angle is important to avoid contamination of cross-shore velocities by the observed strong longshore currents O(1 m s^{-1}). Shore parallel was determined by averaging over ±50 m alongshore [see *Thornton and Guza*, 1986] with an estimated uncertainty of ±2° resulting in errors of <±4 cm s^{-1}.

For the first run on each day the sled was towed by the Coastal Research Amphibious Buggy (CRAB) to its farthest offshore location seaward of the bar (~160 m from the shoreline). A forklift on the beach pulled the sled shoreward 10–30 m for subsequent measurement runs that are referred to in the text by sequential numbers within each day. Each data run was nominally 1 hour, and seven to eight runs were made across a transect during each day spanning the high tide during this period.

Waves and mean water level were measured using an array of five pressure sensors mounted on the sled. Directional wave spectra were also acquired using a linear array of 10 pressure sensors in 8 m depth. Additionally, a 13-element cross-shore array of pressure sensors was used to measure wave heights spanning the width of the surf zone [*Elgar et al.*, 1998]. The fixed array was located ~25 m to the north of the sled transect. These data were continuously sampled at 2 Hz. Video observations were used to measure the fraction of wave breaking along the same transect using the method of *Lippmann and Holman* [1991].

Meteorological information of wind and atmospheric pressure were recorded simultaneously at the seaward end of the 600 m long FRF pier and atop the FRF building in front of the pier. The bathymetry was measured daily using the CRAB, and depth contours were found to be nearly straight and parallel for the 3 days under consideration.

4. Results and Discussion

Measured undertow flows are maximum on top and on the shoreward slope of the bar, with increasing magnitude from October 10 to 12 as wave forcing increased with the approach of a storm (Figure 1). The vertical structure over this region is the classic parabolic shape associated with strong wave-breaking turbulence [*Svendsen*, 1984; *Stive and Wind*, 1986]. In the inner trough the return flow is weak, and almost no vertical structure is seen. At the seaward slope of the bar, observed profiles on October 10 (Figure 1a) are nearly uniform with depth. Significant bottom roughness in the trough of the barred profiles related to the development of lunate and long-crested megaripples as a result of the strong longshore currents [*Thornton et al.*, 1998] is found here. The bar migrated offshore (0 (20 m)) between October 10 and 12, which *Gallagher et al.* [1998] associated with the strong undertow.

Model-data comparisons are evaluated by calculating absolute and relative rms errors. Absolute percent error has dimensional units and is defined by

$$\varepsilon_{\text{abs}} = \sqrt{\frac{1}{N}\sum_{i=1}^{N}(P_i - O_i)^2}, \quad (13)$$

where P_i is model prediction, O_i is the observed quantity, and N is the number of observations. The relative percent error is calculated by

$$\varepsilon_{\text{rel}} = 100\left[\sqrt{\frac{1}{N}\sum_{i=1}^{N}\left(\frac{P_i - O_i}{O_i}\right)^2}\right] \quad (14)$$

and weights the difference between model predictions and observations against a measure of expectation that is represented by the observation. This statistic is not well behaved for small O_i, which sometimes is the case for observed mean cross-shore velocities. Thus measurements smaller than the in situ determined offsets (± 1 cm s^{-1}) are excluded from (14). In section 4.1, the optimized wave transformation model is described first and is then used to predict the surface mass flux, setup, and vertical profiles of the undertow, including contributions from surface rollers.

4.1. Wave Transformation

The rms wave height is approximated by $H_{\text{rms}} = \sqrt{8\sigma^2}$, where σ^2 is the variance calculated from the surface elevation time series. Surface elevation was calculated by Fourier transforming a 1 hour pressure record, applying a linear wave theory transfer function to the complex Fourier amplitudes in the frequency domain, band-pass filtering by zeroing coefficients outside the range of interest (0.05 Hz $< f <$ 0.5 Hz), and inverse transforming to obtain the surface elevation time series.

The sensitivity of the models for surface mass flux, setup, and undertow to errors associated with the use of a random wave transformation model [*Lippmann et al.*, 1996] is investigated by comparing the model results with results using measured wave heights interpolated with cubic splines. The difference between model output and data interpolation methods is shown in Figure 2 for the first run of October 11, which has the largest ε_{rel} (7%).

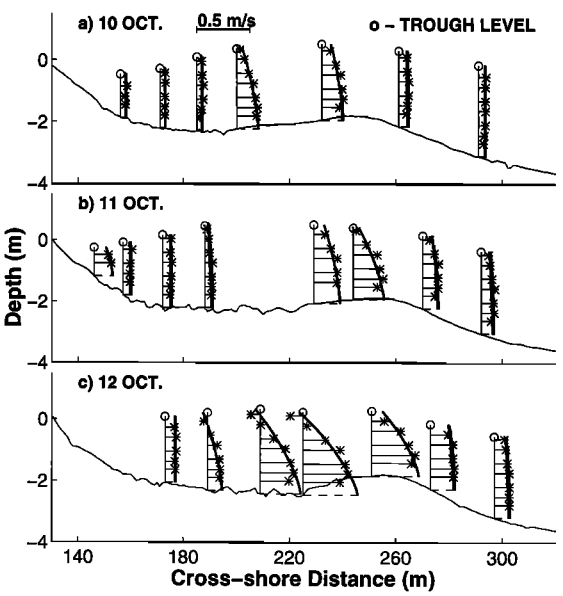

Figure 1. Measured (asterisks) and rms best fit model-predicted (equation (10)) vertical profiles of mean cross-shore return currents (heavy line) superposed on bottom profiles with mean trough level indicated by open circles for the entire period being examined. Models runs were performed for each profile on the transect as they were measured at different times. Mass flux inferred from the measured undertow was used along with optimal coefficients for the wave model and constant eddy viscosity in (10).

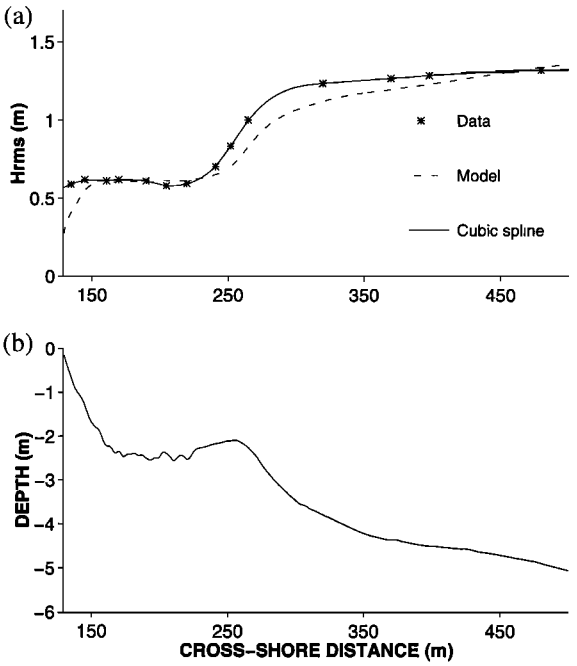

Figure 2. (a) *Lippmann et al.*'s [1996] "worst case" model prediction of H_{rms} versus cross-shore distance (dash-dotted line) compared with cubic spline interpolation (solid line) of observations (asterisks) for the first run of October 11. (b) The bottom profile.

A plot of measured versus modeled H_{rms} for the 3 days analyzed (October 10–12) shows good agreement (Figure 3). The mean ε_{rel} is 5% for all runs, with largest errors at any cross-shore position within 12%. Best fit values for γ and ε_{rel} are summarized in Table 1. In general, the transformation model represents measured wave heights well.

4.2. Surface Mass Flux

The inferred surface mass flux is obtained by numerically integrating the observed cross-shore mean currents from the bottom to the trough level and is compared with model estimates (equation (4)). Here q_r is determined from the cali-

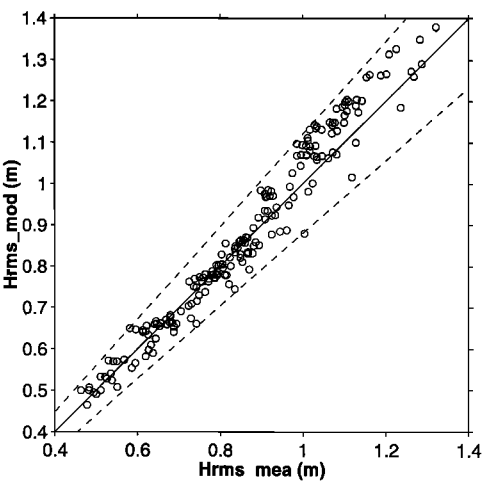

Figure 3. Predicted (*Lippmann et al.*'s [1996] model) versus observed H_{rms}. The solid line represents perfect agreement, and the dashed lines represent the $\pm 10\%$ error bounds.

Table 1. Best Fit Model Parameters for the *Lippmann et al.* and Lippmann and Thornton Models

Model		Wave Transformation[a]		Roller[b]		
Day	Run	γ	Error, %	B	ψ	Error, %
10	1	0.33	2.3	0.70	1.3	2.0
10	2	0.32	4.9	0.60	1.6	3.8
10	3	0.32	4.5	0.60	1.2	3.5
10	4	0.32	4.9	0.70	1.1	5.2
10	5	0.32	4.1	0.65	1.7	4.2
10	6	0.31	4.1	0.75	1.7	4.7
10	7	0.31	5.0	0.75	1.9	4.3
11	1	0.32	7.0	0.85	1.4	7.5
11	2	0.33	4.7	0.65	1.7	6.5
11	3	0.33	4.3	0.70	1.1	7.3
11	4	0.33	3.9	0.65	1.2	5.7
11	5	0.32	4.8	0.60	1.7	3.8
11	6	0.32	4.1	0.85	1.2	7.3
11	7	0.32	5.5	0.70	1.9	3.4
11	8	0.31	6.5	0.85	1.8	5.0
12	1	0.34	5.9	0.90	1.3	3.8
12	2	0.33	5.1	0.80	1.6	7.8
12	3	0.34	5.2	0.80	1.3	9.0
12	4	0.34	4.1	0.80	1.1	8.2
12	5	0.34	4.6	0.75	1.3	7.8
12	6	0.35	5.8	0.65	1.7	5.3
12	7	0.34	5.8	0.95	1.4	7.0
		0.33[c]	4.9[c]	0.75[c]	1.3[c]	5.6[c]

[a]*Lippmann et al.* [1986] model.
[b]Lippmann and Thornton (submitted manuscript, 1998) model.
[c]Mean values.

brated Lippmann and Thornton (submitted manuscript, 1998) model, and q_w is determined first using linear wave theory and then using nonlinear theory for comparison. Predicted q_r are dependent on the percentage of breaking waves in this model. For the 22 profiles examined, best fit values of B range from 0.60 to 0.95 and of ψ range from 1.1 to 1.9 (Table 1), and the error between the observed and modeled percentage of breakers is $\varepsilon_{rel} = 5.6\%$. An example of the observed and predicted percentage of breakers is shown in Figure 4 for the third run of October 12, which has the largest rms error (9%).

Inferred and predicted surface mass fluxes using linear wave theory are compared for the entire ensemble in Figure 5. Because of significant changes associated with wave-breaking characteristics, the data have been divided into four regions: seaward slope of the bar, shoreward slope of the bar, trough, and foreshore. The ε_{rel} between observations and predictions using only q_w, given by linear theory, is 40%. Including the mass flux contribution from wave rollers, q_r, improves the overall agreement ($\varepsilon_{rel} = 28\%$). Largest values of q_r occur at the shoreward slope of the bar (Figure 5b), where wave breaking is most intense. In this region, q_r is, on average, 72% of q_w but can be as large as 144% (fourth run of October 12). This is in accordance with earlier model studies [*Svendsen*, 1984; *Dally and Brown*, 1995] but contrary to *Masselink and Black* [1995], who contend on the basis of the results from field experiments at two near-planar beaches that the roller contribution to the mass transport is of secondary importance.

The impact of using nonlinear stream function wave theory [*Dean*, 1974] to calculate q_w is examined next as it was shown to give more accurate results with monochromatic laboratory wave data [*Dally and Brown*, 1995]. For the field data examined here, there is little difference between the use of linear or stream function theory, with linear wave theory giving values on average 8% larger (Figure 6).

Errors in surface mass flux predictions could also arise from the misfit in estimating wave heights with a transformation model. The rms relative error in mass flux calculated using the *Lippmann et al.* [1996] model–predicted H_{rms} compared with

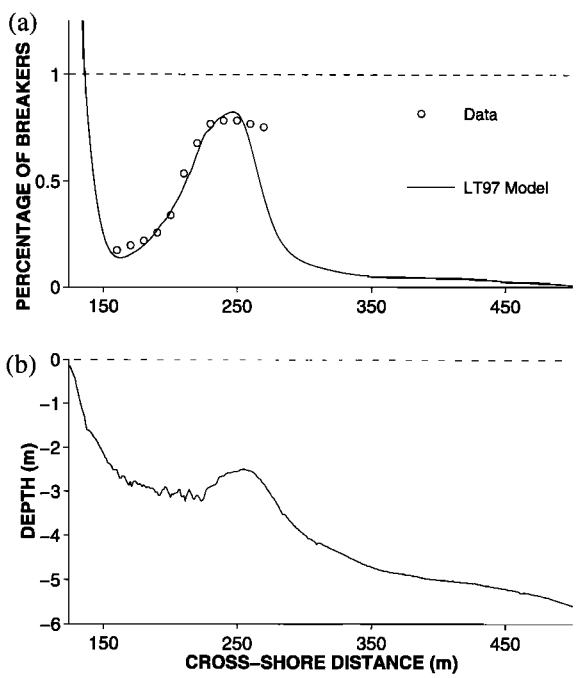

Figure 4. (a) Lippmann and Thornton (submitted manuscript, 1998) model predictions (solid line) and observed (open circles) percentage of waves breaking versus cross-shore distance for the third run of October 12. (b) The bottom profile.

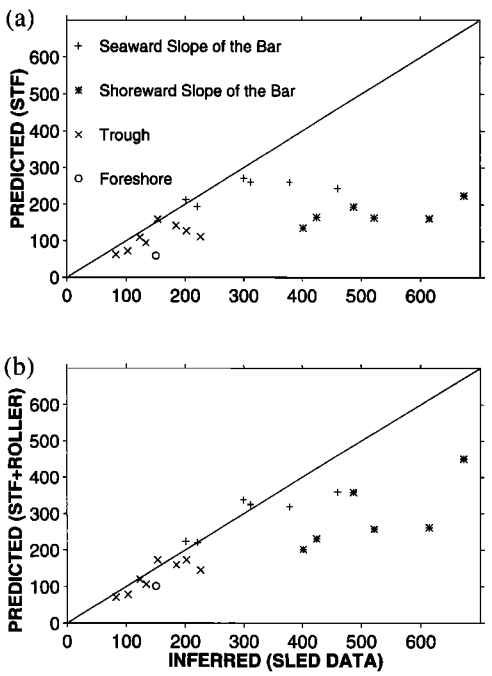

Figure 5. (a) Measured ($\rho U_r h_t$) versus linear wave theory predicted surface mass flux (q_w, only) for the entire ensemble of 22 runs (upper panel). (b) The effect of including contributions from wave rollers ($q_w + q_r$).

using the cubic spline H_{rms} measurements for all runs is 9%, with a maximum relative error of 19.5% (third run of October 12). These results suggest that the surface mass flux is not overly sensitive to the choice of the random wave transformation model. The differences in observed and predicted undertow are not believed to be associated with large-scale, three-dimensional circulation cells, as measured bathymetry was essentially uniform alongshore during the period being analyzed and no qualitative evidence of stationary rip currents was observed in the video.

4.3. Setup

Setup is calculated using a finite centered difference method to solve (12) numerically, with the condition that the setup is assumed to be zero at the most offshore grid point. Contributions from each term of (12) are examined for the fourth run of October 12 (Figure 7), which corresponds to the most energetic period. The cross-shore gradient of the momentum flux associated with wave rollers is calculated using the Lippmann and Thornton (submitted manuscript, 1998) model, the radiation stress term is calculated using linear wave theory, and the momentum flux of the current (ρU_r^2) is estimated by applying cubic splines to measured depth-integrated cross-shore mean return flow. The largest contributions are due to the radiation stress and roller terms. The momentum flux of the current, although generally an order of magnitude smaller than the other terms, cannot be neglected, as it can be of the same order as the sum of the larger terms.

The effects on setup using contributions from the roller momentum flux and using nonlinear wave theory to calculate the radiation stress are examined with one example from each day (Figure 8). The effect of the roller is to redistribute momentum laterally into the trough of the bar, shifting the point where the setup begins onshore [*Nairn et al.*, 1990]. This shift has a significant impact on the setup/setdown profile within the surf zone. Nonlinear stream function wave theory predicts less radiation stress and as a result less setdown, although the use of nonlinear wave theory does not appear to alter the setup profile significantly (Figure 8).

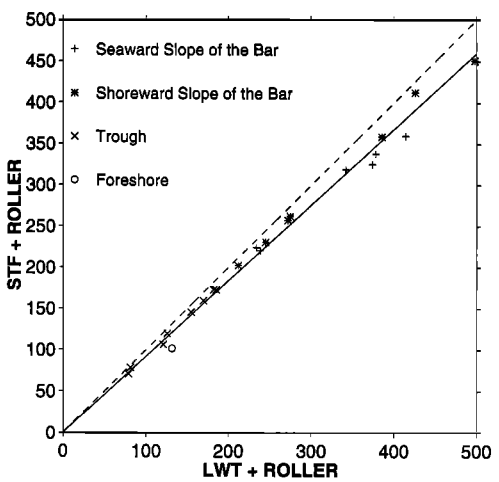

Figure 6. Comparison between predicted surface mass flux ($q_w + q_r$) given by linear (LWT) and stream function [*Dean*, 1974] (STF) wave theories. The dashed line represents perfect agreement, and the solid line represents a linear regression with a slope of 0.92.

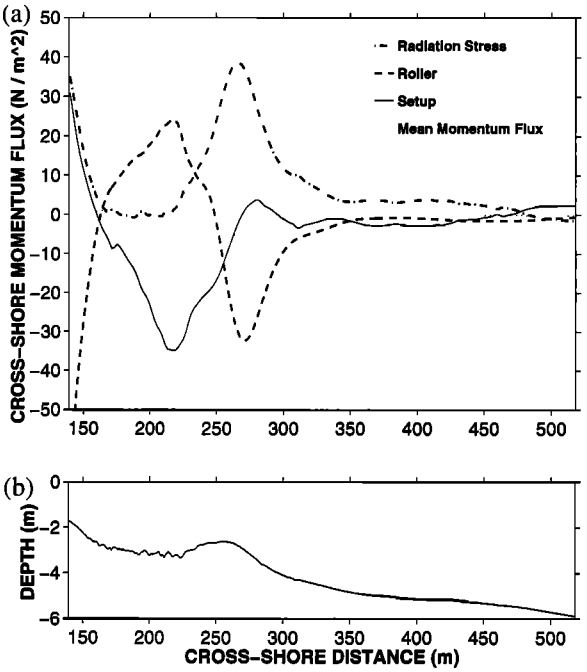

Figure 7. (a) Terms of the momentum balance equation (12) versus cross-shore distance for the fourth run of October 12. (b) The bottom profile.

4.4. Undertow

4.4.1. Cross-shore variation of the eddy viscosity. An implicit assumption of the closure model used in the undertow solution is that the eddy viscosity coefficient μ is proportional to turbulence intensity. Conceptually, large cross-shore varia-

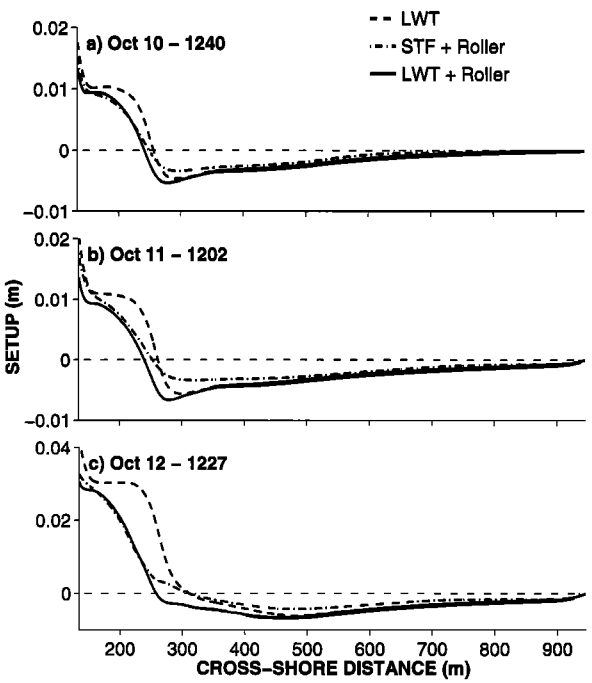

Figure 8. Setup calculated using linear wave theory (dashed line), stream function theory with roller (dash-dotted line), and linear wave theory with roller (solid line) versus cross-shore distance for the fourth run of each day.

Table 2. Observed Wave, Tide, Undertow, and Viscosity

Day	Run	Significant Wave Height H_0, m	Peak Frequency f_p, Hz	Peak Direction α_0, deg	Tide	Depth-Averaged Undertow U_{obs}, m s^{-1}	rms Best Fit Eddy Viscosity μ, m^2 s^{-1}
10	1	1.70	0.171	44	0.40	0.06	0.500
10	2	1.81	0.162	38	0.79	0.08	0.500
10	3	1.81	0.162	38	0.98	0.16	0.058
10	4	1.68	0.152	36	0.77	0.14	0.017
10	5	1.68	0.152	36	0.44	0.05	0.500
10	6	1.44	0.162	24	0.04	0.05	0.500
10	7	1.44	0.162	24	−0.12	0.05	0.500
11	1	2.11	0.142	18	0.22	0.10	0.240
11	2	1.88	0.142	16	0.64	0.12	0.250
11	3	1.75	0.142	17	0.86	0.19	0.033
11	4	1.70	0.142	18	0.92	0.19	0.049
11	5	1.70	0.142	18	0.85	0.05	0.063
11	6	1.70	0.142	18	0.62	0.08	0.500
11	7	1.60	0.142	16	0.32	0.07	0.500
11	8	1.60	0.142	16	0.03	0.15	0.140
12	1	1.91	0.162	18	0.05	0.13	0.130
12	2	2.29	0.142	12	0.34	0.20	0.240
12	3	2.29	0.142	12	0.71	0.30	0.032
12	4	2.32	0.142	10	0.83	0.30	0.036
12	5	2.32	0.142	10	0.84	0.20	0.035
12	6	2.35	0.142	10	0.69	0.07	0.020
12	7	2.35	0.142	10	0.42	0.10	0.500

Best-fit eddy viscosity values are based on using splined H_{rms} and observed mean undertow to specify mass transport.

tion of μ is expected throughout the surf zone over a natural barred beach associated with significant changes in wave breaking–generated turbulence. *Haines and Sallenger* [1994], in an earlier field experiment limited to 3 ems over the vertical at this same beach, used a different model for the vertical variation of the undertow and found that the best fit μ for each location varied by more than an order of magnitude across the surf zone (μ = 0.0055 − 0.075 m^2 s^{-1}). *Smith et al.* [1992], on the other hand, applied a constant μ across the surf zone (μ = 0.05 m^2 s^{-1}) and found reasonable agreement with the Delilah data.

To investigate the cross-shore variation of the eddy viscosity, best fit μ (Table 2) were calculated using (10) by minimizing both the ε_{abs} and ε_{rel} in $\langle U(z)\rangle$ at each cross-shore position occupied by the sled (Figure 1). Observed depth-mean undertow velocities U_r and observed splined rms wave heights were used in the calculations to isolate effects due to the choice of μ. For all 22 runs, $\langle\varepsilon_{abs}\rangle$ = 2.2 cm s^{-1} ($\langle\varepsilon_{rel}\rangle$ = 19%) with maximum ε_{abs} = 6.1 cm s^{-1} (ε_{rel} = 44%) for the fourth run of October 12. Here $\langle\varepsilon_{abs}\rangle$ is less than the accuracy of the observations. Using modeled rms wave heights [*Lippmann et al.*, 1996], ε_{abs} = 2.5 cm s^{-1} (ε_{rel} = 22%), which indicates that the vertical profile of the undertow is not sensitive to errors associated with the use of a random wave transformation model. Using the surface mass flux model to estimate U_r results in $\langle\varepsilon_{abs}\rangle$ = 5.1 cm s^{-1} and $\langle\varepsilon_{rel}\rangle$ = 48%, which suggest that the largest errors in the vertical profile of mean undertow are related to the failure of the existing models to predict correctly the surface mass flux in breaking waves.

Models for the vertical structure of the undertow that use an eddy viscosity closure to solve for the turbulent shear stress (Reynolds stress), independent of the choice of boundary conditions and depth dependence of the eddy viscosity, result in a general solution of the form

$$U(z) = U_{ref} + \frac{\langle F(x)\rangle}{\rho\mu} S(z), \tag{15}$$

where U_{ref} is a reference velocity that could be either the depth-averaged undertow [e.g., *Stive and Wind*, 1986] or the velocity at the top of the BBL [e.g., *Svendsen et al.*, 1987]. A nearly uniform vertical profile of undertow, as observed in the inner trough and seaward slope of the bar (Figure 1), requires either no forcing (F = 0) or an infinite eddy viscosity to be reproduced correctly. An example of the spatial distribution of each term and of the total $F(x)$ for the first run of October is shown in Figure 9. The dominance of the setup gradient term is evident, and hence the model predicts offshore directed flow throughout the entire surf zone, which agrees with observations. The modeled total forcing, although small offshore of the bar and within the trough where the undertow was nearly uniform, was never nil within the cross-shore transect occupied by the sled, which was also the case for all the other runs during the period being analyzed. Minimum rms errors over these regions are obtained for large eddy viscosity values (Table 2), with a maximum cutoff level arbitrarily set at μ = 0.5 m^2 s^{-1}. These unrealistically large values of μ are associated with the sensitivity of the eddy viscosity model to small errors in the dynamical forcing, which is calculated as the difference between two large numbers (setup and radiation stress gradients).

The parameterization for the eddy viscosity is of the form $\mu \approx lC$, where l and C are characteristic length and velocity scales [*Battjes*, 1975]. Several dimensionally consistent parameters for μ are found in the literature, such as $(H/2)^2 f$ [*Thornton*, 1970], $h(D/\rho)^{1/3}$ [*Battjes*, 1975], $h\sqrt{gh}$ [*Stive and Wind*, 1986], and [*Haines and Sallenger*, 1994],

$$\frac{(kh)^2}{f}\left(\frac{D}{\rho}\right)^{2/3}$$

where D is dissipation associated with wave breaking. An attempt was made to relate best fit μ with these parameters, after excluding from the ensemble, values of μ that reached the cutoff level (Table 2). No statistically significant correlation at the 95% confidence level was obtained between these parameters and best fit μ. On the bar crest and shoreward slope of the bar the mean undertow profile assumes a parabolic shape, and best fit eddy viscosity approaches a constant value ($\mu \approx 0.04$ m^2 s^{-1}).

4.4.2. Vertical variation of the eddy viscosity. Here the impact both of a depth varying μ_z and of different boundary conditions on the vertical structure of the undertow are investigated. It is expected from laboratory measurements [*Ting and Kirby*, 1994; *Cox and Kobayashi*, 1997] that μ_z should increase from the bottom with a maximum near the surface and with increasing levels of wave breaking–generated turbulence. Several mathematical formulations for the vertical variations of μ_z were investigated, and the three solutions that best agreed with data (constant (10), linear (A6), and quadratic (A11) μ_z are described in the appendix. A comparison among these solutions giving the smallest overall rms errors for the entire ensemble is shown in Figure 10 for the two stations within each day that have largest observed vertical structure of the undertow. The absolute and relative percent errors for the entire ensemble of data for optimally fit values are for μ constant (0.014 m^2 s^{-1} and 14.2), μ_z linear (0.018 m^2 s^{-1}, 14.5), and μ_z quadratic (0.018 m^2 s^{-1}, 14.8). Surprisingly, the smallest errors are for μ constant, though the differences between using linear or quadratic μ_z are small. These results confirm earlier modeling comparisons with laboratory data showing that a depth-dependent eddy viscosity does not substantially improve the description of the vertical structure of the mean undertow [*Svendsen and Buhr Hansen*, 1988; *Nadaoka et al.*, 1989].

The influence of the boundary condition choice on the vertical structure of the mean undertow in the middle layer (using μ constant) is investigated next. Comparison between predictions by (10), which uses the conservation of mass over the vertical and the stress at the trough level as boundary conditions, and by (11), which uses a no-slip condition at the bottom to replace the stress at the trough level as the second boundary condition, is shown in Figure 11 for the same stations used in Figure 10. Again, no significant improvement in the total rms errors between observations and predictions by these two solutions is obtained, although there are noticeable differences in the predicted currents by each model as a function of depth. Equation (10) shows better overall comparison with data, while (11) represents better the structure of the flow in the lower half of the water column. Although models coupling the middle layer and BBL flows (equation (11)) are expected to provide a more realistic description of the undertow structure close to the bed, their applicability to field conditions is still limited by the lack of velocity data near the bed to constrain their free parameters.

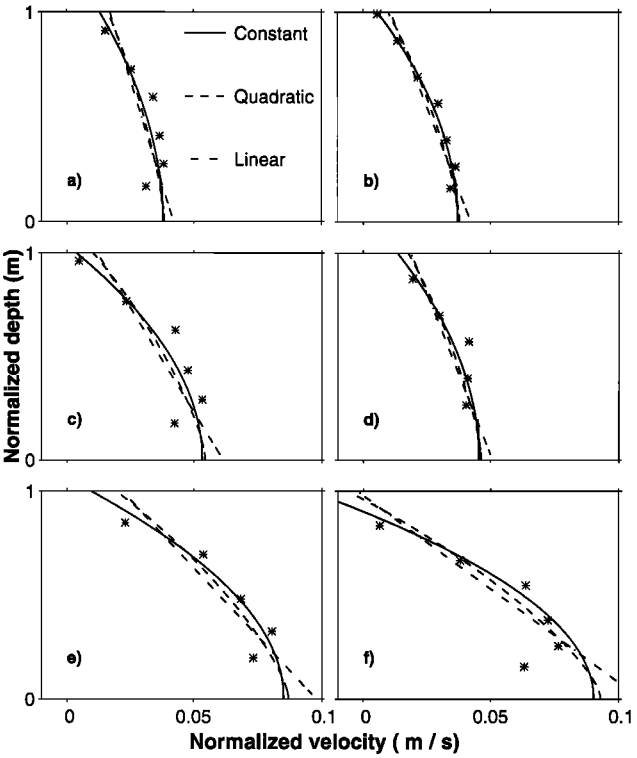

Figure 10. Comparison between measured undertow (asterisks) and predictions using different formulations for the vertical variation of the eddy viscosity with optimally fit coefficients (constant, solid line; linear, dash-dotted line; and parabolic, dashed line) for the (a) third and (b) fourth runs of October 10, the (c) third and (d) fourth runs of October 11, and the (e) third and (f) fourth runs of October 12. Model runs use splined H_{rms} and observed mean undertow to specify mass transport.

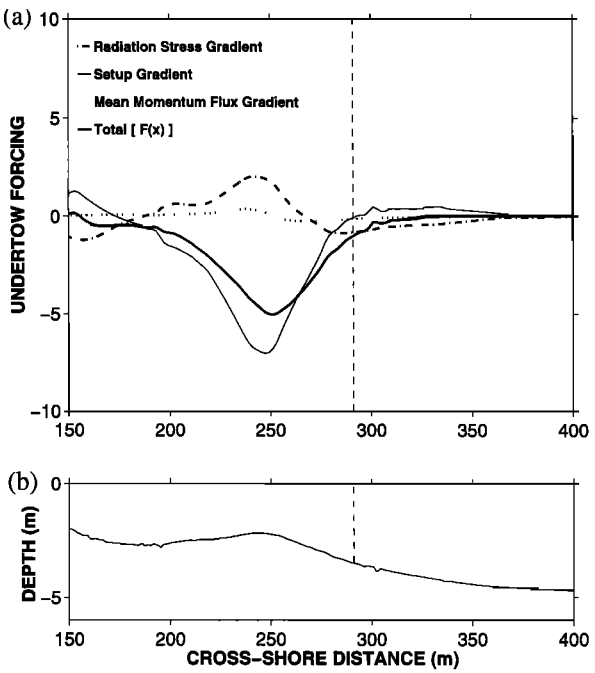

Figure 9. (a) Undertow dynamical forcing terms (equation (6)) versus cross-shore distance for the first run of October 10. (b) The bottom profile. The vertical dashed line indicates the cross-shore position occupied by the sled.

5. Conclusions

The predicted spatial distributions of mean cross-shore current (undertow) over a barred beach are compared with field observations during the Duck94 experiment to quantify the relative importance of contributions from the various terms in

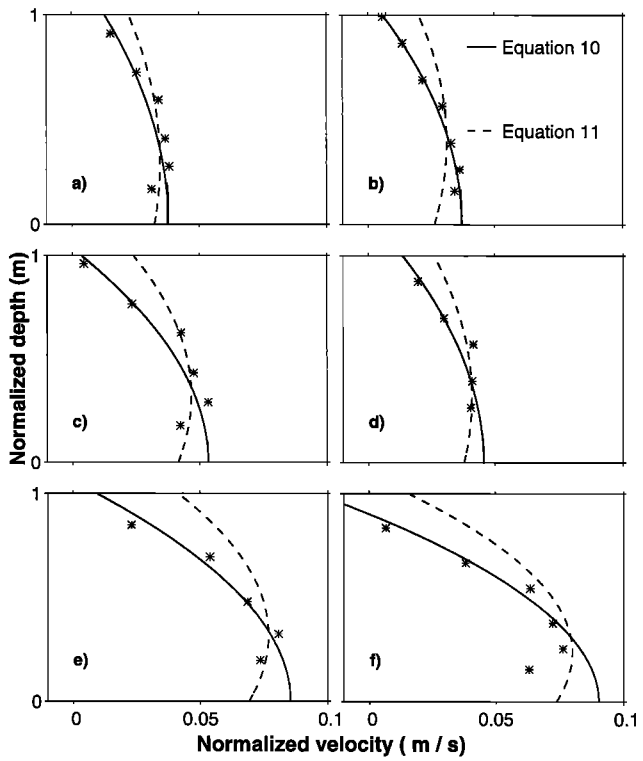

Figure 11. Same as Figure 10 but comparing predictions given by (10) (solid line) and (11) (dashed line).

the cross-shore momentum equation and to identify physical mechanisms not yet incorporated in existing nearshore models.

The largest discrepancies between model predictions and observations of undertow velocities appear to be associated with the failure of existing models to predict correctly the surface mass flux under breaking waves just inside the bar. The surface mass flux model based on potential flow theory contributions from wave rollers is compared with field observations obtained by integrating the measured return flow from the bottom to the wave trough level and assuming conservation of mass over the vertical. It was found that the roller contributions to the mass transport can be larger than the contributions from the organized wave motion when energetic breaking waves are present. Surface mass flux predicted using linear wave theory combined with contributions from wave rollers were 8% larger compared with the solution given by nonlinear stream function wave theory.

Setup (setdown) is a dominant forcing mechanism for the undertow and is calculated from the depth-integrated and time-averaged cross-shore momentum balance. It is found that despite the dominance of the setup (setdown) and radiation stress gradients in this balance the contribution from the convective acceleration of the mean current is significant during energetic wave events. It is also shown that the inclusion of contributions from wave rollers results in an onshore shift of the point where the setup begins, which has a significant impact on the dynamical balance of forces within the surf zone.

The vertical structure of the undertow is modeled using a turbulent eddy viscosity closure, and depth-dependent eddy viscosity formulations are found not to improve the agreement with the field data compared with using constant eddy viscosity. On the bar crest and shoreward slope of the bar, where strong wave breaking was observed, the mean undertow profile assumes a parabolic shape, and best fit eddy viscosity approaches a constant value ($\mu \approx 0.04$ m^2 s^{-1}).

The effect of using different boundary conditions to solve for the vertical structure of the mean undertow is investigated by including random waves in the formulations of *Stive and Wind* [1986] and *Svendsen et al.* [1987] by ensemble averaging over the wave distribution (equations (10) and (11)). No significant difference in the total rms errors between observations and predictions is found between these two solutions. Despite the better representation of the undertow structure close to the bed obtained by using (11), which couples the middle layer and BBL flows, its applicability to field conditions is still limited by the lack of velocity data near the bed to constrain its free parameters.

In the inner trough and seaward slope of the bar the measurements show almost no vertical structure for the mean undertow, which would require a local balance between setup gradient and wave forcing ($F = 0$) or a large eddy viscosity ($\mu \rightarrow \infty$) to be properly modeled. Although small, model-predicted forcing was never nil within these regions, so that unrealistically large values of μ are required to model the observed uniform profile of the undertow. These unrealistically large values of μ are associated with the sensitivity of the eddy viscosity model to small errors in the dynamical forcing, which is calculated as the difference between two large numbers (setup and radiation stress gradients).

The absence of both setup measurements and observations of currents close to the bed is a major limitation of the present study. Setup is an integral measure of the dynamic response of the mean water level to cross-shore gradients of momentum fluxes, and its gradient is an important driving force for the undertow within the surf zone. The lack of current measurements close to the bed prevents a quantitative evaluation of the effect of applying different boundary conditions to solve for the vertical profile of the undertow.

Appendix

The solution for the case of an eddy viscosity that varies linearly with depth, as suggested by *Okayasu et al.* [1988], is derived in more detail. Following *Stive and Wind* [1986], the stress at the trough level and conservation of mass over the vertical are used as boundary conditions. The final solutions for other depth-dependent formulations for the eddy viscosities investigated in this study are also included.

A1. Linear: $\mu_z = \alpha + \beta z'$

In this solution a normalized vertical coordinate is introduced:

$$z' = \frac{(z + h)}{h_t},$$

The primes are omitted hereafter for simplicity of notation. Assuming the undertow forcing to be constant over depth and using the eddy viscosity closure for the turbulent shear stress, a solution for the vertical distribution of the mean undertow is obtained by integrating (6) over depth to give

$$\rho\mu_z \frac{\partial U(z)}{\partial z} = \bar{\tau}(z) = F(x)z + C_1, \qquad \text{(A1)}$$

where C_1 is an integration constant that is solved by evaluating (A1) at the bottom ($z = 0$):

$$C_1 = \tilde{\tau}_b \tag{A2}$$

Integrating (A1) a second time and using (A2) gives

$$U(z) = \frac{F(x)}{\rho\beta}\left[z - \frac{\alpha}{\beta}\ln(\alpha + \beta z)\right] + \frac{\tilde{\tau}(z)}{\rho\beta}\ln(\alpha + \beta z) + C_2, \tag{A3}$$

where C_2 is an integration constant that is solved by applying conservation of mass over the vertical to give

$$C_2 = U_r - \frac{F(x)}{\rho\beta}\left(\frac{d_t}{2} - \frac{\alpha}{\beta}C_0\right) - \frac{\tilde{\tau}(z)}{\rho\beta}C_0, \tag{A4}$$

where

$$C_0 = \frac{\alpha}{\beta d_t}\ln\left(\frac{\alpha + \beta d_t}{\alpha}\right) + \ln(\alpha + \beta d_t) - 1. \tag{A5}$$

Substituting (A4) in (A3), the final solution for the vertical profile of the undertow is given by

$$U(z) = U_r + \frac{F(x)}{\rho\beta}\left\{\left(z - \frac{d_t}{2}\right) - \frac{\alpha}{\beta}[\ln(\alpha + \beta z) + C_0]\right\} + \frac{\tilde{\tau}(z)}{\rho\beta}[\ln(\alpha + \beta z) - C_0], \tag{A6}$$

where $\beta > 0$.

A2. Quadratic: $\mu_z = \alpha + \beta(z)^{1/2}$

In this solution,

$$U(z) = U_r + \frac{F(x)}{\rho\beta}\left[M_1(z) - \frac{4d_6^{3/2}}{15} - \frac{\alpha^2}{\beta^2}M_3\right] + \frac{\tilde{\tau}(z)}{\rho\beta}\left[M_2(z) + \frac{2\alpha d_t^{-1/2}}{\beta} - M_3\right], \tag{A7}$$

where

$$M_1(z) = \frac{2}{3}z^{3/2} - \frac{\alpha}{\beta}z + \frac{2A^2}{\beta^2}z^{1/2} - \frac{2\alpha^3}{\beta^3}\ln(\alpha + \beta z^{1/2}), \tag{A8}$$

$$M_2(z) = 2z^{1/2} - 2\alpha\ln(\alpha + \beta z^{1/2}), \tag{A9}$$

$$M_3 = \frac{1}{\beta^3 d_t}\left\{\frac{4\beta^3}{3}d_t^{3/2} + \alpha\beta^2 d_t + 2\alpha(\alpha^2 - \beta^2)\ln(\alpha + \beta d_t^{1/2}) - \alpha[2\ln(\alpha) + 1]\right\}, \tag{A10}$$

where $\beta > 0$.

A3. Parabolic: $\mu_z = \alpha + \beta[z - (z)^2]$

This parabolic form for the vertical variation of the eddy viscosity was suggested by *Roelvink and Reniers* [1994] and observed by *Cox and Kobayashi* [1997] with LDV in a laboratory experiment on regular waves spilling on a rough plane slope.

$$U(z) = U_r + \frac{F(x)}{\rho\beta\psi}\left[N_1(z) - \frac{N_3}{d_t}\right] + \frac{\tilde{\tau}(z)}{\rho\beta\psi}\left[N_2(z) + -\frac{N_4}{d_t}\right], \tag{A11}$$

where

$$N_1(z) = \beta\tanh^{-1}\left(\frac{2\beta z - \beta}{\psi}\right) - \frac{\psi}{2}\ln[\alpha + \beta(z - z^2)], \tag{A12}$$

$$N_2(z) = 2\beta\tanh^{-1}\left(\frac{2\beta z - \beta}{\psi}\right), \tag{A13}$$

$$N_3 = \psi d_t - (2\alpha + \beta d_t)\tanh^{-1}\left(\frac{2\beta d_t - \beta}{\psi}\right) - 2\alpha\tanh^{-1}\left(\frac{\beta}{\psi}\right) - \frac{\psi d_t}{2}\ln[\alpha + \beta(d_t - d_t^2)] + N_4, \tag{A14}$$

$$N_4 = (2\psi d_t - \beta)\tanh^{-1}\left(\frac{2\beta d_t - \beta}{\psi}\right) - \beta\tanh^{-1}\left(\frac{\beta}{\psi}\right) - \frac{\psi}{2}\ln\left[\frac{\alpha + \beta(d_t - d_t^2)}{\alpha}\right], \tag{A15}$$

$$\psi = \sqrt{\beta^2 + 4\alpha\beta}. \tag{A16}$$

In (A1)–(A16) the eddy viscosity μ_z is a function of two nondimensional parameters (α and β). The value of the eddy viscosity at the bottom ($\mu_{z=0}$) is given by α, which in this study is assumed to be represented by the molecular viscosity because of the lack of reliable measurements of currents close to the bed under field conditions to better constrain this value. The solution within the middle layer does not, however, change significantly if the assumed constant eddy viscosity within the BBL [*Putrevu and Svendsen*, 1993] is used for α.

Acknowledgments. This research was funded by the Office of Naval Research, Coastal Sciences Program, under contract N00114-95-AF-002. The authors wish to express their appreciation to all those who participated in the Duck94 experiment, particularly the staff of the U.S. Army Field Research Facility under the direction of B. Birkemeier. The cross-shore array of pressure sensor data was provided by S. Elgar and R. T. Guza. In addition, special appreciation is expressed to Jim Stockel and R. Wyland, Naval Postgraduate School, for their role in the acquisition and processing of wave and current data. The authors thank Jurjen Battjes for helpful suggestions and the anonymous reviewers for their constructive criticisms.

References

Battjes, J. A., Modelling of turbulence in the surf zone, paper presented at Symposium on Modelling Techniques, Am. Soc. of Civ. Eng., San Francisco, Calif., 1975.

Cox, D. T., and N. Kobayashi, A kinematic undertow model with a logarithmic boundary layer, *J. Waterw. Port Coastal Ocean Div. Am. Soc. Civ. Eng., 123*, 354–360, 1997.

Dally, W. R., and C. A. Brown, A modeling investigation of the breaking wave roller with application to cross-shore currents, *J. Geophys. Res., 100*, 24,873–24,883, 1995.

Dally, W. R., and R. G. Dean, Suspended sediment transport and beach profile evolution, *J. Waterw. Port Coastal Ocean Div. Am. Soc. Civ. Eng., 110*, 15–33, 1984.

Dean, R. G., Evaluation and development of water wave theories for engineering applications, *Spec. Rep. 1*, U.S. Army Waterw. Exp. Stn., Vicksburg, Miss., 1974.

Deigaard, R., A note on the three-dimensional shear stress distribution in a surf zone, *Coastal Eng., 20*, 157–171, 1993.

Deigaard, R., P. Justesen, and J. Fredsoe, Modeling of undertow by a one-equation turbulence model, *Coastal Eng., 15*, 431–458, 1991.

Dyhr-Nielsen, M., and T. Sørensen, Sand transport phenomena on coasts with bars, paper presented at 12th Coastal Engineering Conference, Am. Soc. of Civ. Eng., Washington, D. C., 1970.

Elgar, S., R. T. Guza, B. Raubenheimer, T. H. C. Herbers, and E. L. Gallagher, Spectral evolution of shoaling and breaking waves on a barred beach, *J. Geophys. Res.*, *103*, 15,797–15,805, 1998.

Gallagher, E. L., S. Elgar, and R. T. Guza, Observations of sand bar evolution on a natural beach, *J. Geophys. Res.*, *103*, 3203–3215, 1998.

Garcez Faria, A. F., E. B. Thornton, T. P. Stanton, C. V. Soares, and T. C. Lippmann, Vertical profiles of longshore currents and related bed shear stress and bottom roughness, *J. Geophys. Res.*, *103*, 3217–3232, 1998.

Haines, J. W., and A. H. Sallenger Jr., Vertical structure of mean cross-shore currents across a barred surf zone, *J. Geophys. Res.*, *99*, 14,223–14,242, 1994.

Lippmann, T. C., and R. A. Holman, Phase speeds and angle of breaking waves measured with video techniques, paper presented at Coastal Sediments 91, Am. Soc. Civ. Eng., Seattle, Wash., 1991.

Lippmann, T. C., A. H. Brookins, and E. B. Thornton, Wave energy transformation on natural profiles, *Coastal Eng.*, *27*, 1–20, 1996.

Longuet-Higgins, M. S., and R. W. Stewart, Radiation stresses in water waves: A physical discussion, with applications, *Deep Sea Res.*, *11*, 529–562, 1964.

Masselink, G., and K. P. Black, Magnitude and cross-shore distribution of bed return flow measured on natural beaches, *Coastal Eng.*, *25*, 165–190, 1995.

Nadaoka, K., and T. Kondoh, Laboratory measurements of velocity field structure in the surf zone by LDV, *Coastal Eng. Jpn.*, *25*, 125–145, 1982.

Nadaoka, K., M. Hino, and Y. Koyano, Structure of the turbulent flow field under breaking waves in the surf zone, *J. Fluid Mech.*, *204*, 359–387, 1989.

Nairn, R. B., J. A. Roelvink, and H. N. Southgate, Transition zone width and implications for modeling surf zone hydrodynamics, paper presented at 22nd Coastal Engineering Conf., Am. Soc. of Civ. Eng., Delft, Netherlands, 1990.

Okayasu, A., T. Shibayama, and K. Horikawa, Vertical variation of undertow in surf zone, paper presented at 21st Coastal Engineering Conf., Am. Soc. of Civ. Eng., Costa del Sol-Malaga, Spain, 1988.

Putrevu, U., and I. A. Svendsen, Vertical structure of the undertow outside the surf zone, *J. Geophys. Res.*, *98*, 22,707–22,716, 1993.

Rivero, F. J., and A. S. Arcilla, On the vertical distribution of $\langle \tilde{u}\tilde{w} \rangle$, *Coastal Eng.*, *25*, 137–152, 1995.

Roelvink, J. A., and A. J. H. M. Reniers, Upgrading of a quasi-3D hydrodynamic model, paper presented at Mast-II Overall Workshop, Gregynog, Wales, U. K., 1994.

Smith, J. K., I. A. Svendsen, and U. Putrevu, Vertical structure of the nearshore current at Delilah: Measured and modeled, paper presented at 23rd Coastal Engineering Conference, Am. Soc. of Civ. Eng., Venice, Italy, 1992.

Stive, M. J. F., and H. G. Wind, A study of radiation stress and set-up in the nearshore region, *Coastal Eng.*, *6*, 1–25, 1982.

Stive, M. J. F., and H. G. Wind, Cross-shore mean flow in the surf zone, *Coastal Eng.*, *10*, 325–340, 1986.

Svendsen, I. A., Mass flux and undertow in a surf zone, *Coastal Eng.*, *8*, 347–365, 1984.

Svendsen, I. A., and J. Buhr Hansen, Cross-shore currents in surf-zone modelling, *Coastal Eng.*, *12*, 23–42, 1988.

Svendsen, I. A., H. A. Schäffer, and J. Buhr-Hansen, The interaction between the undertow and the boundary layer flow on a beach, *J. Geophys. Res.*, *92*, 11,845–11,856, 1987.

Thornton, E. B., Variation of longshore currents across the surf zone, paper presented at 12th Coastal Engineering Conference, Am. Soc. of Civ. Eng., London, 1970.

Thornton, E. B., and R. T. Guza, Transformation of wave height distribution, *J. Geophys. Res.*, *88*, 5925–5938, 1983.

Thornton, E. B., and R. T. Guza, Surf zone longshore currents and random waves: Field data and models, *J. Phys. Oceanogr.*, *16*, 1165–1178, 1986.

Thornton, E. B., J. L. Swayne, and J. R. Dingler, Small-scale morphology related to waves and currents across the surf zone, *Mar. Geol.*, *145*, 173–196, 1998.

Ting, F. C. K., and J. T. Kirby, Observation of undertow and turbulence in a laboratory surf zone, *Coastal Eng.*, *24*, 51–80, 1994.

A. F. Garcez Faria, Marinha-Directoria de Hidrografiea e Navegacao, Rio de Janeiro 24048, Brazil.

T. C. Lippmann, Byrd Polar Research Center, Ohio State University, Columbus, OH 43210-1002.

T. P. Stanton and E. B. Thornton, Oceanography Department, Naval Postgraduate School, Monterey, CA 93940-5000. (thornton@oc.nps.navy.mil)

(Received August 23, 1998; revised December 14, 1999; accepted March 22, 2000.)